Nitsche extended finite element method of a Ventcel transmission problem with discontinuities at the interface

Daniela Capatina[*], Fabien Caubet[†], Marc Dambrine[‡], Rodrigo Zelada[§]

May 23, 2024

Abstract

The objective of this work is to study a diffusion equation with non-standard transmission conditions, which include discontinuities and the Ventcel boundary conditions at the interface. To handle jumps and means of the flux and test-functions, we use broken Sobolev spaces. We present a Nitsche finite element approach and compare it with a discontinuous Galerkin method. Consistency, stability and *a priori* error estimates are proven and numerically verified.

Keywords: Finite element method; Nitsche method; Ventcel boundary condition; asymptotic model.

AMS Classification: 65N12, 65N15, 65N30, 35S15, 35C20.

1 Introduction

Motivations. In this work, we consider a heat diffusion problem with an interface. Motivated by the need to optimise the shape of a heat exchanger between two fluids, we find ourselves in a situation where the wall separating them is very thin. In an actual simulation, it would be extremely expensive to mesh at the scale of the thickness of this wall. Therefore, we consider the model resulting from an asymptotic analysis with a small parameter ϵ representing the thickness of the interface. The particularity of the studied problem is that it involves an interface on which the transmission conditions have jumps and involve surface scattering. These conditions, also known as *Ventcel conditions* (see [15]), have the particularity in this model of involving the small parameter ϵ. The final goal being the optimisation of the shape of this interface, we want to develop a numerical method that is robust with respect to this small parameter and that allows the use of iterative solvers.

Setting of the problem. Let us present the precise problem under study. Let B an open bounded domain of $\mathbb{R}^d$, with $d = 2, 3$. Let Ω_1, Ω_2 be a partition of B. We set $\Gamma := \partial\Omega_1 \cap \partial\Omega_2$ the interface between Ω_1 and Ω_2. We define $\Omega := B \setminus \Gamma$. Here and in the following, the subscript $_i$ stands for $_1$ and $_2$. The boundaries of Ω_i are respectively described by $\partial\Omega_i =: \Gamma_{i,\mathrm{D}} \cup \Gamma_{i,\mathrm{N}} \cup \Gamma$ (see Figure 1).

We introduce the following notation for the jump and mean at the interface. Let v any function defined on Ω, and $v_i := v|_{\Omega_i}$ its restriction to Ω_i. Then the jump and mean of v at Γ are denoted by $[\cdot]$ and $\langle\cdot\rangle$ respectively and defined as follows:

$$[v] := v_2 - v_1 \text{ on } \Gamma, \quad \text{and} \quad \langle v\rangle := \frac{v_1 + v_2}{2} \text{ on } \Gamma.$$

[*]Université de Pau et des Pays de l'Adour, E2S UPPA, CNRS, LMAP, UMR 5142, 64000 Pau, France. daniela.capatina@univ-pau.fr

[†]fabien.caubet@univ-pau.fr

[‡]marc.dambrine@univ-pau.fr

[§]rodrigo.zelada-mancini@univ-pau.fr

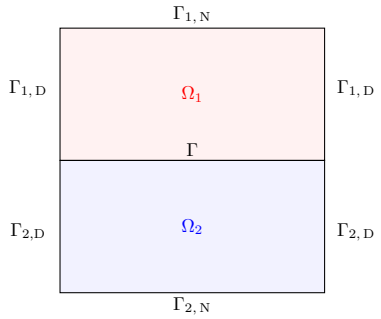

Figure 1: Illustration of the domain Ω.

We define $\Gamma_{\mathrm{D}} := \Gamma_{1,\mathrm{D}} \cup \Gamma_{2,\mathrm{D}}$ and similarly, $\Gamma_{\mathrm{N}} := \Gamma_{1,\mathrm{N}} \cup \Gamma_{2,\mathrm{N}}$. We assume here that $\overline{\Gamma} \cap \overline{\Gamma}_{\mathrm{N}} = \emptyset$ and that $\overline{\Gamma} \cap \overline{\Gamma}_{\mathrm{D}} \neq \emptyset$. Other geometrical configurations could also be treated by changing the functional spaces. Let $\kappa_1, \kappa_2, \epsilon, \alpha$ be strictly positive constants and let $\epsilon > 0$ fixed. We then consider the following interface problem:

$$\begin{cases} -\operatorname{div}(\kappa_i \nabla u_i) &= G & \text{in } \Omega_i,\ i=1,2, \\ u_i &= u_{i,\mathrm{D}} & \text{on } \Gamma_{i,\mathrm{D}},\ i=1,2, \\ \kappa \dfrac{\partial u}{\partial \mathrm{n}} &= 0 & \text{on } \Gamma_{\mathrm{N}}, \\ \left\langle \kappa \dfrac{\partial u}{\partial \mathrm{n}} \right\rangle &= -\dfrac{1}{\epsilon}[u] + \dfrac{\bar{f}}{\epsilon} + f & \text{on } \Gamma, \\ \left[\kappa \dfrac{\partial u}{\partial \mathrm{n}} \right] &= \alpha\epsilon \Delta_\tau \langle u \rangle + \alpha\epsilon \bar{g} + g & \text{on } \Gamma, \end{cases} \tag{1.1}$$

where $G \in \mathrm{L}^2(\Omega)$, $u_{i,\mathrm{D}} \in \mathrm{H}^{1/2}_{00}(\Gamma_{i,\mathrm{D}})$ for $i = 1,2$, $f, \bar{f}, g, \bar{g} \in \mathrm{L}^2(\Gamma)$ and Δ_Γ is the *Laplace-Beltrami operator* (see, e.g. [11]). Let $u_{\mathrm{D}} \in \mathrm{H}^{1/2}_{00}(\Gamma_{1,\mathrm{D}} \cup \Gamma_{2,\mathrm{D}})$ given by $u_{\mathrm{D}}|_{\Gamma_{i,\mathrm{D}}} := u_{i,\mathrm{D}}$ on $\Gamma_{i,\mathrm{D}}$ $(i = 1,2)$, where

$$\mathrm{H}^{1/2}_{00}(\Gamma_{1,\mathrm{D}} \cup \Gamma_{2,\mathrm{D}}) := \{ v|_{\Gamma_{1,\mathrm{D}} \cup \Gamma_{2,\mathrm{D}}},\, v \in \mathrm{H}^{1/2}(\partial\Omega),\, v|_{\partial\Omega \setminus (\Gamma_{1,\mathrm{D}} \cup \Gamma_{2,\mathrm{D}})} = 0 \}.$$

Remark 1.1. *This problem can be seen as a generalization of the following one studied in [2]:*

$$\begin{cases} -\operatorname{div}(\kappa_i \nabla u_i) &= G & \textit{in } \Omega_i,\ i=1,2, \\ u &= u_{\mathrm{D}} & \textit{on } \Gamma_{\mathrm{D}}, \\ \kappa \dfrac{\partial u}{\partial \mathrm{n}} &= 0 & \textit{on } \Gamma_{\mathrm{N}}, \\ \left\langle \kappa \dfrac{\partial u}{\partial \mathrm{n}} \right\rangle &= -\dfrac{1}{\epsilon}[u] & \textit{on } \Gamma, \\ \left[\kappa \dfrac{\partial u}{\partial \mathrm{n}} \right] &= 0 & \textit{on } \Gamma. \end{cases}$$

Aim of the present work. At the continuous level, such a boundary problem can be analysed using *broken Sobolev spaces*. Their numerical implementation implies to double the degrees of freedom at the interface, which is not always possible in calculation codes such as FEniCS and FreeFem++. We mention here the work [1] of Allaire *et al.* in a related context of shape optimisation of an interface where they overcome the difficulty by using a penalisation/extension method for the numerical approximation, without any error estimates.

In the present work, we aim to carry out the numerical analysis of the previous problem and provide *a priori* error estimates. However, our problem presents an additional difficulty: the presence of the small parameter ϵ which appears at different scales in the transmission conditions.

We first highlight that the classical discontinuous Galerkin method is not robust with respect to this small parameter. The conditioning of the associated linear system blows up when ϵ tends towards 0. The reason is that the solution of the limit problem, obtained when ϵ tends towards 0, does not belong to the same variational space. For this reason, we then propose a modification of this first method.

We are inspired by Nitsche's method, which was introduced in [14] to weakly impose Dirichlet boundary conditions. It was adapted by Hansbo and Hansbo in [10] for transmission problems where the interface is not aligned with the mesh. In [6], it was used for a scattering problem with Ventcel boundary conditions. It has to be noticed that in [6], there is also a small parameter ϵ but it does not appear at the order $\frac{1}{\epsilon}$ in the transmission conditions which makes the problem different. We propose here a method based on [12] to deal with these conditioning problems, adapted to Nitsche's method with Robin-Fourier conditions.

Organisation of the paper. The paper is organised as follows. Section 2 is devoted to the introduction of the model problem, the functional spaces and the weak formulation. Section 3 explains the discrete framework, with the finite element approximation and numerical illustrations, where conditioning problems are discussed. In Section 4, the Nitsche method is proposed to solve the conditioning problems and numerical examples are presented. In Section 5, conclusions and prospects for future work are discussed.

2 The continuous problem

2.1 Functional setting

Let $k \in \mathbb{N}^*$. It is useful to introduce the broken Sobolev space

$$V^k := \{v \in \mathrm{L}^2(\Omega); v_i := v|_{\Omega_i} \in \mathrm{H}^k(\Omega_i),\ i = 1, 2\},$$

which endowed with the norm

$$\|v\|_{k,\Omega_1\cup\Omega_2} := \left(\|v_1\|^2_{k,\Omega_1} + \|v_2\|^2_{k,\Omega_2}\right)^{1/2}$$

is a Hilbert space. Its subspace

$$V^k_\Gamma := \{v \in V^k; v_i \in \mathrm{H}^1_0(\Gamma) \cap \mathrm{H}^k(\Gamma),\ i = 1, 2\}$$

endowed with the norm

$$\|v\|_{V^k_\Gamma} := \left(\|\kappa^{1/2} v\|^2_{k,\Omega_1\cup\Omega_2} + \|(\alpha\epsilon)^{1/2} \langle v\rangle\|^2_{k,\Gamma} + \|\epsilon^{-1/2}[v]\|^2_{k-1,\Gamma}\right)^{1/2}$$

is also a Hilbert space. Let

$$V^k_{\Gamma,u_\mathrm{D}} := \{v \in V^k_\Gamma; v = u_\mathrm{D} \text{ on } \Gamma_\mathrm{D}\} \quad \text{and} \quad V^k_{\Gamma,0} := \{v \in V^k_\Gamma; v = 0 \text{ on } \Gamma_\mathrm{D}\}.$$

Finally, in the case $k = 1$, it is useful to introduce:

$$\|v\| := \left(\|\kappa^{1/2}\nabla v\|^2_{0,\Omega_1\cup\Omega_2} + |\|(\alpha\epsilon)^{1/2} \langle\nabla_\tau v\rangle\||^2_{0,\Gamma}\right)^{1/2} \quad \text{and} \quad |||v||| := \left(\|v\|^2 + \|\epsilon^{-1/2}[v]\|^2_{0,\Gamma}\right)^{1/2}.$$

Due to the trace theorem on Γ and on Ω_i for $i = 1, 2$, the space $V^1_{\Gamma,0}$ endowed with the norm $|||\cdot|||$ is a Hilbert space.

Remark 2.1. *In the case where* $\overline{\Gamma} \cap \overline{\Gamma}_{\mathrm{D}} = \emptyset$ *and* $\overline{\Gamma} \cap \overline{\Gamma}_{\mathrm{N}} \neq \emptyset$*, one assumes that the domain* Ω *is such that* $\tau_\Gamma = \mathrm{n}_{\Gamma_{\mathrm{N}}}$ *on* $\partial\Gamma$*, where* τ_Γ *is the unit tangent vector to* Γ *and normal to* $\partial\Gamma$*, and takes as functional space*

$$V^1_\Gamma = \{v \in V^1; v_i \in \mathrm{H}^1(\Gamma),\ i = 1, 2\}. \tag{2.1}$$

In the case with mixed boundary conditions that intersect the interface, that is $\overline{\Gamma} \cap \overline{\Gamma}_{j,\mathrm{D}} \cap \overline{\Gamma}_{j,\mathrm{N}} \neq \emptyset$*, where* $j \in \{1, 2\}$*, one also assumes* $\tau_\Gamma = \mathrm{n}_{\Gamma_{\mathrm{N}}}$ *on* $\partial\Gamma$*, and then considers*

$$V^1_\Gamma = \{v \in V^1; v_i \in \mathrm{H}^1(\Gamma), i = 1, 2, v_j = 0 \text{ on } \overline{\Gamma} \cap \overline{\Gamma}_{j,\mathrm{D}} \cap \overline{\Gamma}_{j,\mathrm{N}}\}.$$

Finally, in the case where $\overline{\Gamma} \cap \overline{\Gamma}_{\mathrm{D}} = \overline{\Gamma} \cap \overline{\Gamma}_{\mathrm{N}} = \emptyset$*, one uses the functional space* (2.1)*.*

2.2 Variational formulation

For a fixed value of ϵ, one defines the bilinear forms

$$\begin{aligned} b(u, v) &:= \sum_{i=1}^{2} \int_{\Omega_i} \kappa_i \nabla u_i \cdot \nabla v_i \,\mathrm{d}x + \int_\Gamma \alpha\epsilon \nabla_\tau \langle u \rangle \cdot \nabla_\tau \langle v \rangle \,\mathrm{d}s, \\ c(u, v) &:= \int_\Gamma \frac{1}{\epsilon} [u][v] \,\mathrm{d}s. \end{aligned}$$

Then, one considers the following variational formulation of Problem (1.1):

$$\left\{ \begin{array}{l} \text{Find } u \in V^1_{\Gamma, u_{\mathrm{D}}} \text{ such that} \\ \forall v \in V^1_{\Gamma,0}, \quad a(u, v) = l(v), \end{array} \right. \tag{2.2}$$

where

$$\begin{aligned} a(u, v) &:= b(u, v) + c(u, v), \\ l(v) &:= \int_\Omega Gv \,\mathrm{d}x + \int_\Gamma (f[v] + g \langle v \rangle) \,\mathrm{d}s + \int_\Gamma \left(\frac{1}{\epsilon} \bar{f}[v] + \alpha\epsilon \bar{g} \langle v \rangle \right) \mathrm{d}s. \end{aligned}$$

In the next theorem, without loss of generality, we assume that $u_{\mathrm{D}} = 0$, otherwise consider $\tilde{u}_{\mathrm{D}} \in \mathrm{H}^1(\Omega_1 \cup \Omega_2)$ such that $\tilde{u}_{\mathrm{D}} = u_{\mathrm{D}}$ on Γ_{D} and then define $\tilde{u} := u - \tilde{u}_{\mathrm{D}}$ which belongs to $V^1_{\Gamma,0}$.

Theorem 2.2 (Well-posedness)**.** *Let* $G \in \mathrm{L}^2(\Omega)$*,* $f \in \mathrm{L}^2(\Gamma)$*,* $g \in \mathrm{L}^2(\Gamma)$ *and* $u_{\mathrm{D}} = 0$*. Then Problem* (2.2) *has a unique solution* $u \in V^1_{\Gamma,0}$*. Furthermore, the following estimate holds:*

$$|||u||| \leq C \max_{i=1,2} \kappa_i^{-1/2} \left(\|G\|_{0,\Omega} + \|g\|_{0,\Gamma} + \alpha\epsilon \|\bar{g}\|_{0,\Gamma} \right) + \epsilon^{1/2} \|f\|_{0,\Gamma} + \epsilon^{-1/2} \|\bar{f}\|_{0,\Gamma}, \tag{2.3}$$

with a constant $C > 0$ *depending only on the domains* Ω_1 *and* Ω_2*.*

Proof. Clearly, $a(\cdot, \cdot)$ is bilinear and symmetric and $l(\cdot)$ is linear. Note that $a(\cdot, \cdot)$ is a scalar product on $V^1_{\Gamma,0}$, of corresponding norm $|||\cdot|||$, so it is continuous and coercive with respect to this norm, of continuity and coercivity constants equal to 1. As regards the continuity of $l(\cdot)$, we first note that the Poincaré inequality yields, for any $v \in V^1_{\Gamma,0}$, that

$$\|v\|_{0,\Omega_i} \leq C_P(\Omega_i) \kappa_i^{-1/2} \|\kappa_i^{1/2} \nabla v\|_{0,\Omega_i}, \quad i = 1, 2,$$

while the trace theorem together with the Poincaré inequality yield:

$$\| \langle v \rangle \|_{0,\Gamma} \leq \frac{1}{2} \sum_{i=1}^{2} C_T(\Omega_i) \sqrt{1 + C_P(\Omega_i)^2} \kappa_i^{-1/2} \|\kappa_i^{1/2} \nabla v\|_{0,\Omega_i}.$$

The $|||\cdot|||$ - continuity of $l(\cdot)$ follows thanks to the Cauchy-Schwarz inequality:

$$|l(v)| \leq |||v||| \left(C \max_{i=1,2} \kappa_i^{-1/2} \left(\|G\|_{0,\Omega} + \|g\|_{0,\Gamma} + \alpha\epsilon\|\bar{g}\|_{0,\Gamma} \right) + \epsilon^{1/2}\|f\|_{0,\Gamma} + \epsilon^{-1/2}\|\bar{f}\|_{0,\Gamma} \right).$$

By virtue of the Lax-Milgram theorem, Problem (2.2) has a unique solution in $V^1_{\Gamma,0}$. The estimate (2.3) is classically obtained by testing the weak problem with $v = u$ and by using the previous bound. □

2.3 A remark on the limit problem as $\epsilon \to 0$ at the continuous level

Formally, by making ϵ tend towards 0, Problem (1.1) becomes

$$\left\{ \begin{array}{rll} -\operatorname{div}(\kappa_i \nabla u_i^0) &= G & \text{in } \Omega_i,\ i = 1, 2, \\ u_i^0 &= u_{i,\mathrm{D}} & \text{on } \Gamma_{\mathrm{D}},\ i = 1, 2, \\ \kappa \dfrac{\partial u^0}{\partial n} &= 0 & \text{on } \Gamma_{\mathrm{N}}, \\ [u^0] &= \bar{f} & \text{on } \Gamma, \\ \left[\kappa \dfrac{\partial u^0}{\partial n} \right] &= g & \text{on } \Gamma. \end{array} \right. \tag{2.4}$$

The natural functional space in order to study Problem (2.4) is the following affine space:

$$U_{\tilde{f}} := \{ v \in V^1_{\Gamma,u_{\mathrm{D}}}; [v] = \tilde{f} \text{ on } \Gamma \}.$$

Once endowed with the norm $\|v\|_{U_0} := \|\kappa^{1/2}\nabla v\|_{0,\Omega_1\cup\Omega_2}$,, the subspace $U_0 := \{ v \in V^1_{\Gamma,0}; [v] = 0 \text{ on } \Gamma \}$ is a Hilbert space. Hence one can prove that Problem (2.4) has a unique solution $u^0 \in U_{\tilde{f}}$: the proof is a mere adaptation of a Laplacian problem with mixed boundary conditions, considering that instead of the Dirichlet boundary condition we have the jump condition in the functional space.

Note that the functional spaces associated to Problem (1.1) and Problem (2.4) are different, which suggests numerical difficulties when ϵ tends to 0. This last point is discussed in the following section.

3 Discontinuous Lagrange finite elements approximation

For the sake of simplicity, one assumes that the domain Ω is a polyhedron in $\mathbb{R}^d$ and Γ a finite union of hyperplanes. Let $\mathcal{T}_h$ be a regular simplicial mesh of Ω: there exists a parameter $\sigma > 0$ such that, for all $K \in \mathcal{T}_h$,

$$\frac{h_K}{\rho_K} \leq \sigma,$$

where h_K is the diameter of K and ρ_K is the diameter of the largest ball contained in K. We define $h := \max_{K\in\mathcal{T}_h} h_K$ the mesh size. Assume that the mesh is always aligned with the interface Γ, i.e., each $K \in \mathcal{T}_h$ is a subset of only one set Ω_i. Finally, we define $\mathcal{T}_h^i := \{K \in \mathcal{T}_h; K \subset \Omega_i\}$, $i = 1, 2$.

Let $\mathcal{F}_h$ be the set of faces of $\mathcal{T}_h$, $\mathcal{F}_{h,\Gamma}$ the set of faces situated on Γ and $\mathcal{T}_{h,\Gamma}$ the set of elements which have one face on Γ. Let h_F be the diameter of the face $F \in \mathcal{F}_{h,\Gamma}$ (in $d = 2$, h_F coincides with the 1-Hausdorff measure of F). Let $k \in \mathbb{N}^*$ and let

$$P_h^k := \{ v_h \in V^1_\Gamma; v_h|_{\Omega_i} \in \mathcal{C}(\Omega_i), v_h|_K \in \mathbb{P}^k, \forall K \in \mathcal{T}_h \} \quad \text{and} \quad P^k_{h,0} := P_h^k \cap V^1_{\Gamma,0}.$$

In the sequel, we make the additional assumption that the Dirichlet condition u_{D} belongs to $\mathrm{H}^{k+1/2}(\Gamma_{1,\mathrm{D}} \cup \Gamma_{2,\mathrm{D}})$. Let $u_{\mathrm{D},h} \in P_h^k$ denote a nodal interpolation of u_{D} on Γ_{D}. An intuitive and natural discrete formulation of Problem (1.1) is then:

$$\left\{ \begin{array}{l} \text{Find } w_h \in P_h^k, \text{ such that } w_h = u_{\mathrm{D},h} \text{ on } \Gamma_{\mathrm{D}} \text{ and} \\ a(w_h, v_h) = l(v_h), \quad \forall v_h \in P^k_{h,0}. \end{array} \right. \tag{3.1}$$

The aim of this section is first to prove the well-posedness of the discrete formulation and to study the convergence as h tends towards 0 of its solution towards the solution of the continuous problem, and then to study through numerical experiments the behaviour of the discrete scheme, in particular for small values of ϵ.

3.1 Analysis of the discrete formulation

Since $P^k_{h,0} \subset V^1_{\Gamma,0}$, taking $v = v_h \in P^k_{h,0}$ in the variational formulation (2.2) immediately yields the consistency of the discrete problem, stated in the next lemma.

Lemma 3.1 (Consistency of finite element approximation)**.** *Let u be a smooth solution to* (1.1)*. Then*

$$a(u, v_h) = l(v_h), \quad \forall v_h \in P^k_{h,0}. \tag{3.2}$$

The coercivity and continuity are directly inherited from the continuous problem, which permits to obtain the following lemma.

Lemma 3.2 (Discrete coercivity and continuity)**.** *One has that*

$$a(v_h, v_h) = |||v_h|||^2, \quad \forall v_h \in P^k_{h,0} \tag{3.3}$$

and

$$a(w_h, v_h) \leq |||w_h|||\,|||v_h|||, \quad \forall w_h, v_h \in P^k_{h,0}. \tag{3.4}$$

Thus, thanks to the Lax-Milgram theorem, we obtain the following result.

Theorem 3.3. *Problem* (3.1) *has a unique solution $w_h \in P^k_h$.*

Next, in order to obtain the convergence rate of the approximation error, one needs an interpolation estimate. Similarly to [10] but without cut elements (the mesh being aligned with the interface), for each $k \in \mathbb{N}^*$, we consider

$$(\mathcal{I}^k_h)^* v = (\mathcal{I}^k_h v_1)\mathbb{1}_{\Omega_1} + (\mathcal{I}^k_h v_2)\mathbb{1}_{\Omega_2},$$

where $\mathcal{I}^k_h$ is the standard nodal interpolation operator from $\mathrm{H}^{k+1}(\Omega)$ to P^k_h. Using standard interpolation estimates (see [7, Theorem 3.1.6], [4, Theorem 4.4.20]) and the triangle inequality, one gets the following interpolation result.

Lemma 3.4 (Polynomial approximation)**.** *For any $k \in \mathbb{N}^*$ and any $v \in V^{k+1}_{\Gamma,0}$, there exists a constant $C_{\mathrm{ip}} > 0$ independent of h, ϵ, α and κ such that:*

$$|||v - (\mathcal{I}^k_h)^* v||| \leq C_{\mathrm{ip}} h^k \|v\|_{V^{k+1}_\Gamma}. \tag{3.5}$$

Furthermore, we have

$$|||v - (\mathcal{I}^k_h)^* v||| \leq C_{\mathrm{ip}} h^k \left(\|\kappa^{1/2}\nabla v\|^2_{k+1,\Omega_1\cup\Omega_2} + \|(\alpha\epsilon)^{1/2} \langle v \rangle\|^2_{k+1,\Gamma} + h^2 \|\epsilon^{-1/2}[v]\|^2_{k+1,\Gamma} \right)^{1/2}. \tag{3.6}$$

Proof of Lemma 3.4. Let $v \in V^{k+1}_{\Gamma,0}$. Let $K \in \mathcal{T}^i_h$, with $1 \leq i \leq 2$ and $F \in \mathcal{F}_{h,\Gamma}$. By standard interpolation estimates, there exists a constant $C_{\mathrm{ip}} > 0$ independent of h, ϵ, α and κ such that:

$$\begin{aligned} \|\nabla(v_i - \mathcal{I}^k_h v_i)\|_{0,K} &\leq C_{\mathrm{ip}} h^k_K \|v_i\|_{k+1,K}, \\ \|[v] - \mathcal{I}^k_h [v]\|_{0,F} &\leq C_{\mathrm{ip}} h^k_F \|[v]\|_{k,F}, \\ \|\nabla_\tau(\langle v \rangle - \mathcal{I}^k_h \langle v \rangle)\|_{0,F} &\leq C_{\mathrm{ip}} h^k_F \| \langle v \rangle \|_{k+1,F}. \end{aligned}$$

Combining these inequalities leads to:

$$|||v-(\mathcal{I}_h^k)^* v||| \leq C_{\mathrm{ip}} h^k \left(\sum_{i=1}^{2} \sum_{K\in\mathcal{T}_h^i} \|\kappa_i^{1/2} v_i\|_{k+1,K}^2 + \sum_{F\in\mathcal{F}_{h,\Gamma}} \left(\|\epsilon^{-1/2}[v]\|_{k,F}^2 + \|(\alpha\epsilon)^{1/2}\langle v\rangle\|_{k+1,F}^2 \right) \right)^{1/2}$$

which proves (3.5).

Since $[v] \in \mathrm{H}^{k+1}(\Gamma)$, one also has

$$\|[v]-\mathcal{I}_h^k[v]\|_{0,F} \leq C_{\mathrm{ip}} h^{k+1} \|[v]\|_{k+1,F}$$

which, together with the previous inequalities, proves (3.6). □

Therefore, Céa's lemma yields the following *a priori* error estimate.

Theorem 3.5 (Error estimate)**.** *Let $k \in \mathbb{N}^*$ and assume that the solution u of (2.2) belongs to V_Γ^{k+1}. There exists a constant $C_{\mathrm{e}} = 2C_{\mathrm{ip}} > 0$ independent of h, ϵ, α and κ such that*

$$|||\tilde{u}-\tilde{w}_h||| \leq C_{\mathrm{e}} h^k \left(\|\kappa^{1/2}\nabla\tilde{u}\|_{k+1,\Omega_1\cup\Omega_2} + \|(\alpha\epsilon)^{1/2}\langle\tilde{u}\rangle\|_{k+1,\Gamma}^2 + h^2\|\epsilon^{-1/2}[\tilde{u}]\|_{k+1,F}^2 \right)^{1/2} \tag{3.7}$$

where $\tilde{u}_i := u_i - \tilde{u}_{i,\mathrm{D}}$, $\tilde{u} := u - \tilde{u}_{\mathrm{D}}$, $\tilde{w}_h := w_h - \tilde{u}_{\mathrm{D},h}$ with w_h the solution of (3.1), $\tilde{u}_{\mathrm{D}} \in \mathrm{H}^1(\Omega_1\cup\Omega_2)$, $\tilde{u}_{\mathrm{D},h} \in P_h^k$ such that $\tilde{u}_{\mathrm{D}} = u_{\mathrm{D}}$, $\tilde{u}_{\mathrm{D},h} = u_{\mathrm{D},h}$ on Γ_{D} and $\tilde{u}_{\mathrm{D}} = \tilde{u}_{\mathrm{D},h} = 0$ on $\Omega\setminus\Gamma_{\mathrm{D}}$.

Remark 3.6. *The condition $u \in V_\Gamma^{k+1}$ is quite technical to prove but seems to be a reasonable assumption. On the one hand, it was proved in [13] for the case without interface and with the Ventcel condition on the whole boundary (i.e. $\Omega = \Omega_1$, $\Omega_2 = \emptyset$ and $\Gamma = \partial\Omega$). On the other hand, there exist results for standard transmission problems (with zero jumps), see for instance [3]. Then, it might be established that $u \in V_\Gamma^{k+1}$ adapting the previous two proofs under suitable regularity assumptions for the data u_{D}, G, f, g, as well as the interface Γ, but it is not the topic of the present work.*

3.2 Numerical tests

3.2.1 Numerical implementation

We consider the two dimensional case for all the numerical simulations. Moreover, for the sake of simplicity, we consider only the case $k = 1$. The broken Sobolev space $P_{h,0}^k$ can be seen as the usual FE space on Ω, enriched with basis functions associated to the nodes situated on the interface. Thus, the degrees of freedom on Γ are doubled. In order to implement this space, let N_Γ be the number of vertices belonging to Γ and N the number of vertices in the whole mesh of Ω. For each vertex belonging to Γ, of global index i_Γ, we create a copy of new index $\tilde{i}_\Gamma = N + p$, where p is the p^{th} vertex of Γ in ascending order with respect to the index i_Γ of the global mesh, i.e. $i_\Gamma^1 < \ldots < i_\Gamma^p < \ldots < i_\Gamma^{N_\Gamma}$; for instance, $p = 1$ and $p = N_\Gamma$ for the minimum and the maximum index i_Γ, respectively. By convention, we keep the original index i_Γ for a vertex situated on the interface Γ when we look at it from $K \in \mathcal{T}_h^1$ and we use $\tilde{i}_\Gamma$ when we look at it from $K \in \mathcal{T}_h^2$. Now, in the new mesh structure, we allow for duplicate nodes on the interface (same value but different indices in the global mesh). So, if we ignore the Dirichlet boundary conditions, the linear system can be written as $Ax = b$, where A is a square matrix of size $(N + N_\Gamma)$.

As regards the post-processing, we first reconstruct two vectors of size N: U_1 contains the first N values whereas U_2 contains the first N values, but those corresponding to the index i_Γ are replaced by the values corresponding to $\tilde{i}_\Gamma$. Then, we get u_1 and u_2 by restricting U_1 and U_2 to Ω_1 and Ω_2, respectively. The same idea can be employed for a higher polynomial degree $k > 1$ (of course, the indexing will be different due to the additional degrees of freedom).

Finally we precise that all the numerical simulations presented in this article were carried out in `C++`.

3.2.2 Convergence of the method with respect to the mesh size h

In this subsection, the small parameter ϵ is given and fixed. We present some numerical tests in order to validate the error estimate of Theorem 3.5 with respect to h. We consider the two following test-cases.

Case 1. Let us consider $B = [0,1]\times[0,1]$ and a domain $\Omega = \Omega_1 \cup \Omega_2$, where $\Omega_1 = (-0.5, 0.5)\times(0, 0.5)$ and $\Omega_2 = (-0.5, 0.5) \times (-0.5, 0)$ with boundaries $\Gamma = \{y = 0\}$, $\Gamma_{\mathrm{D},1} = \partial\Omega_1 \setminus \Gamma$, $\Gamma_{\mathrm{N},1} = \emptyset$ and $\Gamma_{\mathrm{D},2} = \partial\Omega_2 \setminus \Gamma$, $\Gamma_{\mathrm{N},2} = \emptyset$ as illustrated in Figure 2.

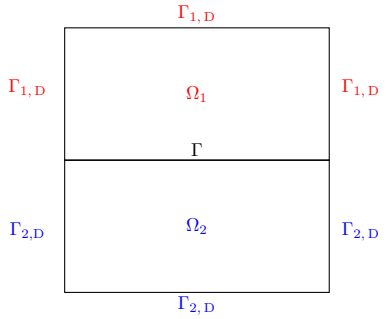

Figure 2: Geometry for case 1

We consider the exact solution:

$$u_1(x,y) = \cos(x+y) \quad \text{and} \quad u_2(x,y) = \sin(x+y),$$

with the corresponding source terms G_1, G_2 and $f(x) = \cos(x)\frac{\kappa_2}{2} - \sin(x)\frac{\kappa_1}{2}$, $\bar{f}(x) = \sin(x) - \cos(x)$, $g(x) = \kappa_1 \sin(x) + \kappa_2 \cos(x)$ and $\bar{g}(x) = \frac{1}{2}\sin(x) + \frac{1}{2}\cos(x)$.

We choose $\kappa_1 = 1$, $\kappa_2 = 10^{-3}$, $\epsilon = 10^{-2}$ and $\alpha = 10^2$. We observe that the method copes well with the case of highly discontinuous coefficients κ_1 and κ_2 when using the arithmetic mean on the interface and not a weighted mean (as employed in [9, 10, 5] for similar problems).

Case 2. As a second example, we consider a curved interface; even if Γ is now different from Γ_h, with a fine meshing at the interface we should retrieve a good convergence (at least for $k = 1$). Let $B = (-1,1) \times (-0.5, 0.5)$, $\Omega_1 = \{(x,y) \in B, x \geq 0, x^2 + y^2 \geq 0.5^2\}$, $\Omega_2 = B \setminus \Omega_1$ with an interface given in polar coordinates by

$$\Gamma = \left\{(0.5\cos\theta, 0.5\sin\theta); \theta \in \left[-\frac{\pi}{2}, \frac{\pi}{2}\right]\right\}$$

and with $\partial\Omega_N = \emptyset$, see Figure 3.

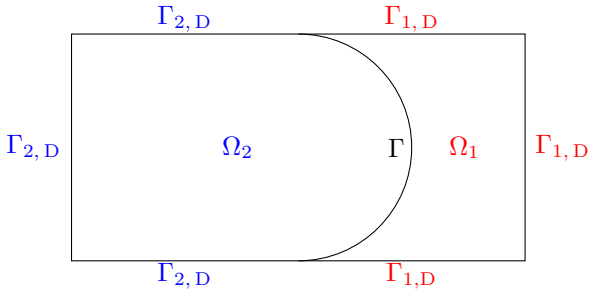

Figure 3: Geometry for case 2

We consider the following exact solution:

$$u_1(x,y) = x\mathrm{e}^y \quad \text{and} \quad u_2(x,y) = y\mathrm{e}^x,$$

with the corresponding source terms G_1, G_2 and with $f = x\mathrm{e}^y\,(\kappa_1+\kappa_1 y)+y\mathrm{e}^x\,(\kappa_2+\kappa_2 x)$, $\bar{f} = x\mathrm{e}^y - y\mathrm{e}^x$, $g = 2\kappa_2 y\mathrm{e}^x(x+1) - 2\kappa_1 x\mathrm{e}^y(y+1)$ and $\bar{g} = -2y\mathrm{e}^x(y^2-3x-1) - 2x\mathrm{e}^y(x^2-3y-1)$. We choose here $\epsilon = \kappa_1 = \kappa_2 = \alpha = 1$.

Numerical results. The energy error $e := |||\tilde{u} - \tilde{w}_h|||$ is split into three parts, $e^2 = e_g^2 + e_\tau^2 + e_j^2$ where

- $e_g := \|\kappa^{1/2}(\nabla\tilde{u} - \nabla\tilde{w}_h)\|_{0,\Omega_1\cup\Omega_2}$ is the gradient error,
- $e_\tau := \|(\alpha\epsilon)^{1/2}\,\langle\nabla_\tau\tilde{u} - \nabla_\tau\tilde{w}_h\rangle\,\|_{0,\Gamma}$ is the tangential error on the interface Γ,
- $e_j := \|\epsilon^{-1/2}[\tilde{u} - \tilde{w}_h]\|_{0,\Gamma}$ is the weighted jump error on Γ.

We validate below the convergence with respect to h. For the first case, h varies between 1.3×10^{-2} to 7.8×10^{-2} and the energy error e varies between 1.8×10^{-3} to 10^{-2}, whereas for the second case h varies between 2.5×10^{-2} to 1.9×10^{-1} and the energy error e varies between 9.8×10^{-3} to 7.6×10^{-2}.

We observe in Figure 4 that in both cases the convergence rate for the energy error e is $\mathcal{O}(h)$, as stated in Theorem 3.5. We obtained similar results for the errors e_g and e_τ.

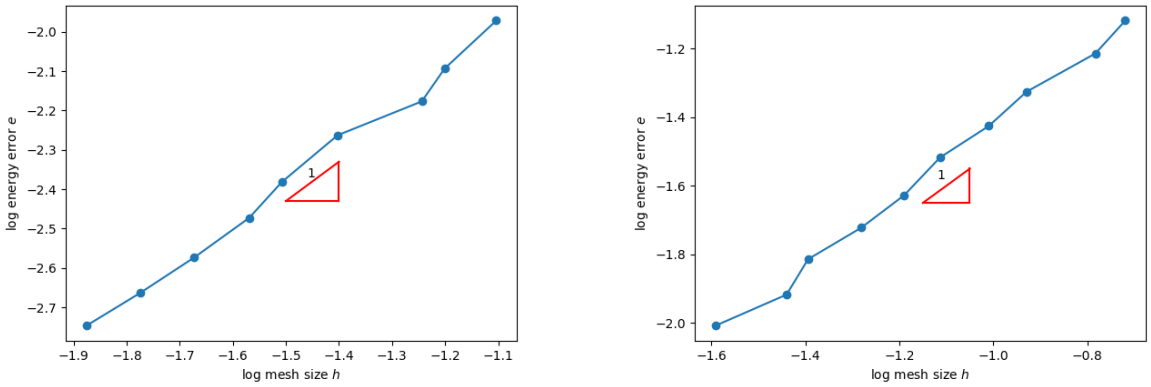

(a) Case 1 with $\epsilon = 10^{-2}$

(b) Case 2 with $\epsilon = 1$

Figure 4: Logarithm plot of the energy error e with respect to the mesh size h

Meanwhile, notice that the convergence rate for the jump error e_j is $\mathcal{O}(h^2)$, as shown in Figure 5. Note that in this case, the gradient error e_g is larger than the jump error e_j, that is why e is of order one.

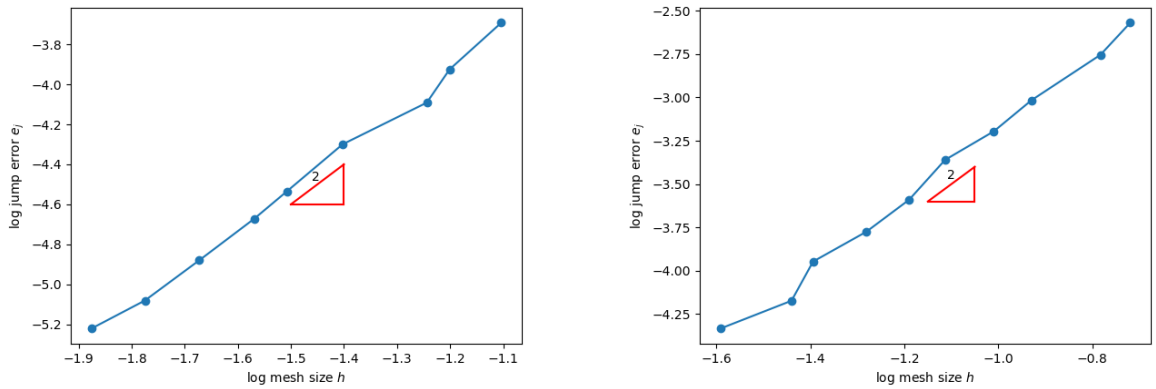

(a) Case 1 with $\epsilon = 10^{-2}$

(b) Case 2 with $\epsilon = 1$

Figure 5: Logarithm plot of the jump error e_j with respect to the mesh size h

The numerical convergence rates are summarized in Table 1.

	Case 1	Case 2
e_g	0.98	1.04
e_τ	0.98	1.06
e_j	1.97	2.05
e	0.99	1.04

Table 1: Convergence rate of each error for the Lagrange discontinuous finite element method

3.2.3 Convergence with respect to ϵ

As previously explained, when ϵ tends towards 0 the transmission boundary condition changes to

$$[u^0] = \bar{f} \text{ on } \Gamma. \tag{3.8}$$

It is then expected to encounter some numerical issues in the limit, since condition (3.8) is included in the functional space whereas our Robin's type interface condition cannot be included in the functional space. In order to illustrate this point, we fix h (which takes different values for each test case) and we let ϵ vary. We can observe in Figure 6 that the energy error e blows up as ϵ decreases towards 0. This is due in partiuclar to the jump error e_j, as shown in Figure 7. One can see in Figure 8 that the tangential gradient error e_τ does not blow up as $\epsilon \to 0$ (and the same behaviour occurs for the gradient error e_g).

3.2.4 Conditioning

We are now interested in the conditioning of the discrete problem in order to explain the bad behaviour of the method when ϵ is too small. We first underline that this has been observed in [12] by Juntunen and Stenberg for the model problem

$$\begin{cases} -\operatorname{div}(\kappa \nabla u) &= G & \text{in } \Omega, \\ \kappa \dfrac{\partial u}{\partial \mathrm{n}} &= -\dfrac{1}{\epsilon} u + \dfrac{\bar{f}}{\epsilon} + f & \text{on } \Gamma. \end{cases}$$

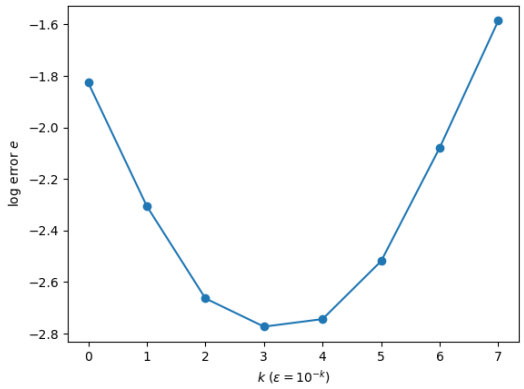

(a) Case 1 with $h = 1.6 \times 10^{-2}$

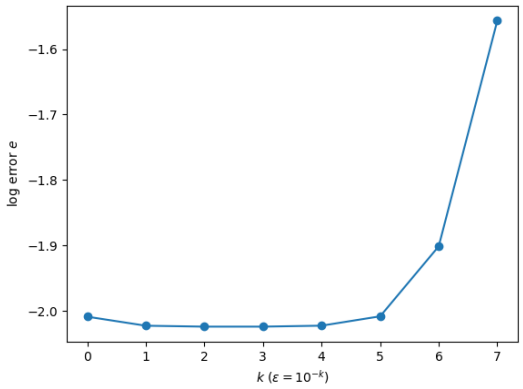

(b) Case 2 with $h = 2.5 \times 10^{-2}$

Figure 6: Logarithm plot of the energy error e with respect to ϵ

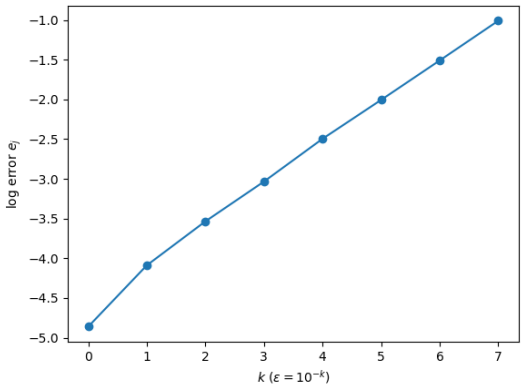

(a) Case 1 with $h = 1.6 \times 10^{-2}$

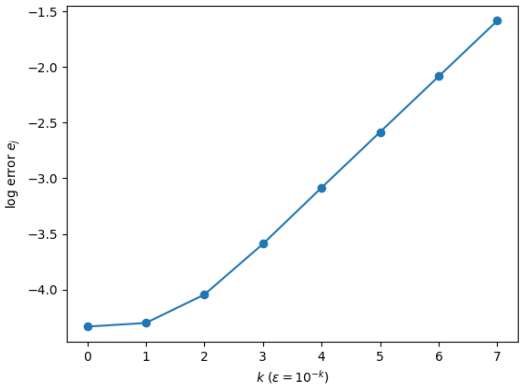

(b) Case 2 with $h = 2.5 \times 10^{-2}$

Figure 7: Logarithm plot of the jump error e_j with respect to ϵ

In this case, they observed that the condition number depends on the value of ϵ as follows:

$$\text{cond} = \mathcal{O}(h^{-2} + (\epsilon h)^{-1}),$$

which leads to

$$\text{cond} = \begin{cases} \mathcal{O}(h^{-2}) & \text{if } \epsilon \geq Ch \\ \mathcal{O}((\epsilon h)^{-1}) & \text{if } \epsilon \leq Ch \end{cases}$$

for some $C > 0$.

For our problem, we also observe that the condition number for the two previous test-cases depends on ϵ, as shown in Figure 9. We considered a fixed value of h, the same parameters as in the previous subsection and plotted the condition number in decimal log scale with respect to $k = -\log_{10} \epsilon$.

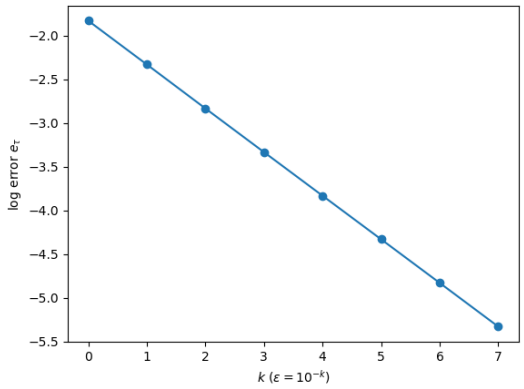

(a) Case 1 with $h = 1.6 \times 10^{-2}$

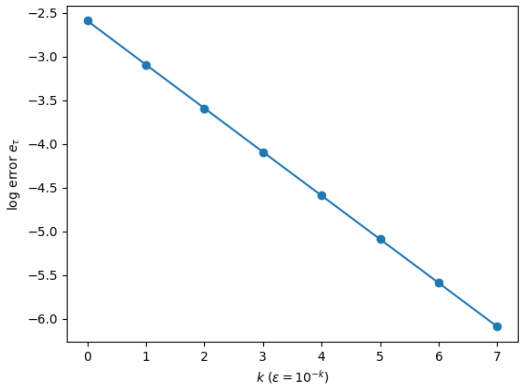

(b) Case 2 with $h = 2.5 \times 10^{-2}$

Figure 8: Logarithm plot of the tangential gradient error e_τ with respect to ϵ

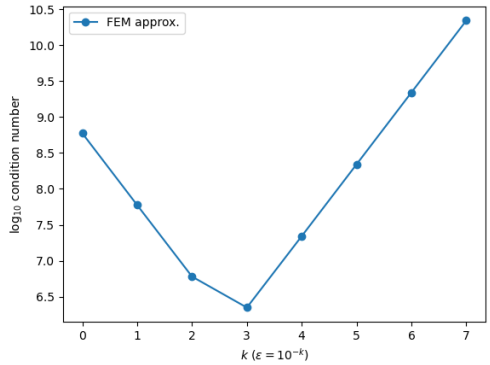

(a) Condition number of case 1 with $h = 3 \times 10^{-2}$

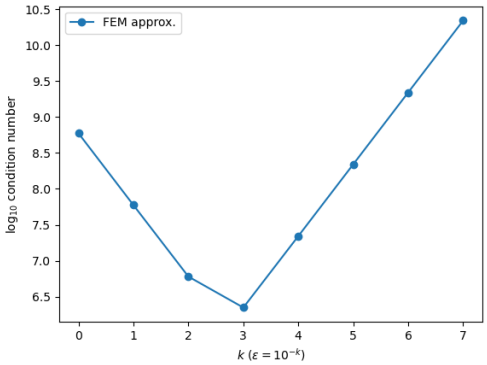

(b) Condition number of case 2 with $h = 5 \times 10^{-2}$

Figure 9: Logarithm plot of the condition number for the two test-cases with respect to ϵ

Despite the consistency property and the optimal convergence with respect to h (at fixed ϵ), the discrete problem gets ill-conditioned when ϵ tends towards 0. Therefore, we propose below another numerical method, which is consistent and coercive, but equally well-conditioned and convergent with respect to ϵ.

4 Modified Nitsche's type formulation

The Nitsche method was originally designed for the weak imposition of Dirichlet boundary conditions in [14]. It was later adapted in [10] to transmission conditions where the mesh is not necessarily aligned with the interface, leading to Nitsche's extended fininite element method (NXFEM). The latter was used in [6] to deal with non-standard transmission conditions involving the Laplace-Beltrami operator.

The main difference between the model problem of [6] and ours is that in [6], the authors considered a

simpler jump condition $[T] = [\chi]$ on Γ, which can be treated by adding to the classical bilinear form the Laplace-Beltrami term. Meanwhile, we consider here a transmission condition of Robin type, involving both the jump and the mean of the normal flux:

$$\left\langle \kappa \frac{\partial u}{\partial \mathrm{n}} \right\rangle = -\frac{1}{\epsilon}[u] + \frac{1}{\epsilon}\bar{f} + f \quad \text{on } \Gamma. \tag{4.1}$$

Therefore, we have to adapt the standard bilinear form used in Nitsche's method.

The general idea of stabilized methods is to add positive (and often, consistent) terms in order to enhance the discrete coercivity with respect to the new energy norm. Here, the issue is not the loss of coercivity but the dependence on ϵ, due to the presence in the energy norm of the jump term, which is multiplied by $\frac{1}{\epsilon}$. So contrarily to stabilized methods, we propose here to subtract a positive term multiplied by a stabilisation parameter depending on both ϵ and h, in view of improving the constant in front of the jump term.

Thus, in order to obtain a consistent and symmetric formulation, we introduce the bilinear and linear forms, defined for any $u_h \in P_h^k$, $v_h \in P_{h,0}^k$ by

$$\begin{aligned} a_h(u_h, v_h) &:= a(u_h, v_h) - \sum_{F \in \mathcal{F}_{h,\Gamma}} \beta_F \left(\left\langle \kappa \frac{\partial u_h}{\partial \mathrm{n}} \right\rangle + \frac{1}{\epsilon}[u_h], \left\langle \kappa \frac{\partial v_h}{\partial \mathrm{n}} \right\rangle + \frac{1}{\epsilon}[v_h] \right)_{0,F}, \\ l_h(v_h) &:= l(v_h) - \sum_{F \in \mathcal{F}_{h,\Gamma}} \beta_F \left(f + \frac{1}{\epsilon}\bar{f}, \left\langle \kappa \frac{\partial v_h}{\partial \mathrm{n}} \right\rangle + \frac{1}{\epsilon}[v_h] \right)_{0,F}, \end{aligned}$$

where the parameter $\beta_F > 0$ will be chosen later. We then consider the following Nitsche's type formulation of Problem (1.1):

$$\begin{cases} \text{Find } u_h \in P_h^k \text{ such that } u_h = u_{\mathrm{D},h} \text{ on } \Gamma_\mathrm{D} \text{ and} \\ a_h(u_h, v_h) = l_h(v_h), \quad \forall v_h \in P_{h,0}^k. \end{cases} \tag{4.2}$$

4.1 Analysis of the discrete formulation

The consistency is straightforward, thanks to (3.2) and to the fact that the transmission condition (4.1), which is weakly imposed in the new formulation, is also strongly satisfied by the continuous solution.

Lemma 4.1 (Consistency of Nitsche's formulation)**.** *Let u be a smooth solution to* (1.1) *and $\beta_F \in \mathbb{R}$, for any $F \in \mathcal{F}_{h,\Gamma}$. Then one has that*

$$a_h(u, v_h) = l_h(v_h), \quad \forall v_h \in P_h^k.$$

In order to show the discrete coercivity, we need a well-known inverse inequality (see for instance [8, Section 1.4.3]). For the sake of clarity, we recall it below and we sketch its proof.

Lemma 4.2 (Inverse inequality)**.** *Let $F \in \mathcal{F}_{h,\Gamma}$ such that $F = \partial K^1 \cap \partial K^2$, with $K^i \in \mathcal{T}_h^i$ for $i = 1, 2$. There exists a constant $C_I > 0$ independent of h, ϵ, α, γ and κ such that:*

$$h_F \left\| \left\langle \kappa \frac{\partial v_h}{\partial \mathrm{n}} \right\rangle \right\|_{0,F}^2 \leq C_I \sum_{i=1}^{2} \|\kappa_i \nabla v_{h,i}\|_{0,K^i}^2, \quad \forall v_h \in P_h^k.$$

Proof. From the discrete trace inequality combined with a standard inverse inequality (see for example [8, Lemma 1.46]), we have for any $w_{h,i} \in (\mathbb{P}^{k-1}(K^i))^d$, $i = 1, 2$, that

$$\frac{1}{h_F} \|\kappa_i w_{h,i}\|_{0,F}^2 \leq \frac{C_{\mathrm{tr}}}{h_{K^i}^2} \|\kappa_i w_{h,i}\|_{0,K^i}^2 .$$

Taking $w_{h,i} = \nabla v_{h,i}$ and noting that $h_F \leq h_{K^i}$ and that $\left|\frac{\partial v_{h,i}}{\partial \mathrm{n}}\right| \leq |\nabla v_{h,i}|$, we immediately obtain:

$$h_F \left\| \left\langle \kappa \frac{\partial v_h}{\partial \mathrm{n}} \right\rangle \right\|_{0,F}^2 \leq \frac{1}{2} \sum_{i=1}^{2} h_F \left\| \kappa \frac{\partial v_{h,i}}{\partial \mathrm{n}} \right\|_{0,F}^2 \leq C_I \sum_{i=1}^{2} \|\kappa_i \nabla v_{h,i}\|_{0,K^i}^2, \quad \forall v_h \in P_h^k$$

with $C_I = C_{\mathrm{tr}}/2$. □

We are next interested in how to choose the stabilization parameter β_F. For this purpose, we write:

$$a_h(v_h, v_h) = b(v_h, v_h) + \frac{1}{\epsilon} \sum_{F \in \mathcal{F}_{h,\Gamma}} (1 - \frac{\beta_F}{\epsilon}) \int_F [v_h]^2 \mathrm{d}s - \sum_{F \in \mathcal{F}_{h,\Gamma}} \beta_F \int_F \left\langle \kappa \frac{\partial v_h}{\partial \mathrm{n}} \right\rangle^2 \mathrm{d}s$$
$$- \sum_{F \in \mathcal{F}_{h,\Gamma}} \frac{2\beta_F}{\epsilon} \int_F \left\langle \kappa \frac{\partial v_h}{\partial \mathrm{n}} \right\rangle [v_h] \, \mathrm{d}s.$$

The Cauchy-Schwarz and the Young inequalities yield that:

$$-2 \sum_{F \in \mathcal{F}_{h,\Gamma}} \frac{\beta_F}{\epsilon} \int_F \left\langle \kappa \frac{\partial v_h}{\partial \mathrm{n}} \right\rangle [v_h] \mathrm{d}s \geq -\frac{1}{2\epsilon} \sum_{F \in \mathcal{F}_{h,\Gamma}} (1 - \frac{\beta_F}{\epsilon}) \|[v_h]\|_{0,F}^2 - \sum_{F \in \mathcal{F}_{h,\Gamma}} \frac{2\beta_F^2}{\epsilon - \beta_F} \left\| \left\langle \kappa \frac{\partial v_h}{\partial \mathrm{n}} \right\rangle \right\|_{0,F}^2 .$$

Plugging this inequality in the definition of $a_h(v_h, v_h)$ leads to:

$$a_h(v_h, v_h) \geq b(v_h, v_h) + \frac{1}{2\epsilon} \sum_{F \in \mathcal{F}_{h,\Gamma}} (1 - \frac{\beta_F}{\epsilon}) \|[v_h]\|_{0,F}^2 - \sum_{F \in \mathcal{F}_{h,\Gamma}} \frac{\beta_F}{h_F} (1 + \frac{2\beta_F}{\epsilon - \beta_F}) h_F \left\| \left\langle \kappa \frac{\partial v_h}{\partial \mathrm{n}} \right\rangle \right\|_{0,F}^2 .$$

Using next Lemma 4.2, we have that:

$$a_h(v_h, v_h) \geq \sum_{K \in \mathcal{T}_h \setminus \mathcal{T}_{h,\Gamma}} \|\kappa^{1/2} \nabla v_h\|_{0,K}^2 + \sum_{K \in \mathcal{T}_{h,\Gamma}} \left(1 - C_I \frac{\beta_F(\epsilon + \beta_F)}{h_F(\epsilon - \beta_F)}\right) \|\kappa^{1/2} \nabla v_h\|_{0,K}^2 + \|\alpha^{1/2} \nabla_\tau \langle v_h \rangle\|_{0,\Gamma}^2$$
$$+ \frac{1}{2\epsilon} \sum_{F \in \mathcal{F}_{h,\Gamma}} (1 - \frac{\beta_F}{\epsilon}) \|[v_h]\|_{0,F}^2. \quad (4.3)$$

Thus, in order to obtain the discrete coercivity of $a_h(\cdot, \cdot)$, it is sufficient to choose β_F such that

$$\beta_F < \epsilon \quad \text{and} \quad \beta_F \frac{\epsilon + \beta_F}{\epsilon - \beta_F} < \frac{h_F}{C_I}. \quad (4.4)$$

Following [12], where a boundary value problem with similar non-standard boundary conditions was considered, we choose $2\beta_F$ as the harmonic mean of ϵ and γh_F, where $\gamma > 0$ is a constant independent of ϵ and of the discretization, that is:

$$\beta_F := \frac{\gamma h_F \epsilon}{\epsilon + \gamma h_F}. \quad (4.5)$$

Then clearly $\beta_F < \epsilon$, while the second inequality of (4.4) translates into $\dfrac{\gamma(\epsilon + 2\gamma h_F)}{\epsilon + \gamma h_F} < \dfrac{1}{C_I}$ and holds true for $\gamma < \dfrac{1}{2C_I}$. With this choice, the bilinear and linear forms can be written as follows:

$$\begin{aligned} a_h(u_h, v_h) &= b(u_h, v_h) + \sum_{F \in \mathcal{F}_{h,\Gamma}} \frac{1}{\epsilon + \gamma h_F} \int_F [u_h][v_h] \mathrm{d}s - \sum_{F \in \mathcal{F}_{h,\Gamma}} \frac{\gamma h_F \epsilon}{\epsilon + \gamma h_F} \int_F \left\langle \kappa \frac{\partial u_h}{\partial \mathrm{n}} \right\rangle \left\langle \kappa \frac{\partial v_h}{\partial \mathrm{n}} \right\rangle \mathrm{d}s \\ &\quad - \sum_{F \in \mathcal{F}_{h,\Gamma}} \frac{\gamma h_F}{\epsilon + \gamma h_F} \int_F \left(\left\langle \kappa \frac{\partial u_h}{\partial \mathrm{n}} \right\rangle [v_h] + \left\langle \kappa \frac{\partial v_h}{\partial \mathrm{n}} \right\rangle [u_h] \right) \mathrm{d}s, \\ l_h(v_h) &= \int_\Omega G v_h \mathrm{d}x + \int_\Gamma (g \langle v_h \rangle + \alpha \epsilon \bar{g} \langle v_h \rangle) \mathrm{d}s \\ &\quad + \sum_{F \in \mathcal{F}_{h,\Gamma}} \frac{1}{\epsilon + \gamma h_F} \int_F (\epsilon f + \bar{f}) \left([v_h] - \gamma h_F \left\langle \kappa \frac{\partial v_h}{\partial \mathrm{n}} \right\rangle \right) \mathrm{d}s. \end{aligned}$$

Remark 4.3. *The case $\gamma = 0$, that is $\beta_F = 0$ for any $F \in \mathcal{F}_{h,\Gamma}$, corresponds to the previous discrete formulation* (3.1)*. The other case when β_F vanishes, that is for $\epsilon = 0$, is more interesting. Contrarily to problem* (3.1)*, we can directly take $\epsilon = 0$ in the new formulation* (4.2) *and obtain the standard Nitsche formulation of the limit problem* (2.4)*.*

Finally, we introduce the following mesh-dependent norm on P_h^k:

$$|||v_h|||_h := \left(\|v_h\|^2 + \sum_{F \in \mathcal{F}_{h,\Gamma}} \frac{1}{\epsilon + \gamma h_F} \|[v_h]\|_{0,F}^2 \right)^{1/2}$$

and we prove below the main result of this subsection, which yields the well-posedness of the discrete problem (4.2) for γ sufficiently small.

Lemma 4.4 (Coercivity and continuity of Nitsche's formulation)**.** *For γ sufficiently small, there exist two positive constants C_{cv}^N, C_{ct}^N independent of h, ϵ, α, γ and κ such that for any $u_h, v_h \in P_{h,0}^k$, one has:*

$$a_h(u_h, v_h) \le C_{\mathrm{ct}}^N |||u_h|||_h |||v_h|||_h \quad \text{and} \quad a_h(v_h, v_h) \ge C_{\mathrm{cv}}^N |||v_h|||_h^2.$$

Proof. The proof of the continuity is standard. The Cauchy-Schwarz inequality yields, for any $u_h, v_h \in P_{h,0}^k$, that

$$\begin{aligned} a_h(u_h, v_h) \le \|u_h\| \|v_h\| &+ \sum_{F \in \mathcal{F}_{h,\Gamma}} \frac{\gamma h_F \epsilon}{\epsilon + \gamma h_F} \left\| \left\langle \kappa \frac{\partial u_h}{\partial \mathrm{n}} \right\rangle \right\|_{0,F} \left\| \left\langle \kappa \frac{\partial v_h}{\partial \mathrm{n}} \right\rangle \right\|_{0,F} \\ &+ \sum_{F \in \mathcal{F}_{h,\Gamma}} \frac{1}{\epsilon + \gamma h_F} \|[u_h]\|_{0,F} \|[v_h]\|_{0,F} \\ &+ \sum_{F \in \mathcal{F}_{h,\Gamma}} \frac{\gamma h_F}{\epsilon + \gamma h_F} \left(\|[u_h]\|_{0,F} \left\| \left\langle \kappa \frac{\partial v_h}{\partial \mathrm{n}} \right\rangle \right\|_{0,F} + \left\| \left\langle \kappa \frac{\partial u_h}{\partial \mathrm{n}} \right\rangle \right\|_{0,F} \|[v_h]\|_{0,F} \right). \end{aligned}$$

Noting that $\dfrac{\gamma h_F \epsilon}{\epsilon + \gamma h_F} \le \gamma h_F$ and that $\dfrac{\gamma h_F}{\epsilon + \gamma h_F} \le \left(\dfrac{\gamma h_F}{\epsilon + \gamma h_F} \right)^{1/2}$ and using again the Cauchy–Schwarz inequality, we further obtain

$$a_h(u_h, v_h) \le \left(\|u_h\|^2 + 2 \sum_{F \in \mathcal{F}_{h,\Gamma}} \left(\frac{1}{\epsilon + \gamma h_F} \|[u_h]\|_{0,F}^2 + \gamma h_F \left\| \left\langle \kappa \frac{\partial u_h}{\partial \mathrm{n}} \right\rangle \right\|_{0,F}^2 \right) \right)^{1/2}$$

$$\times \left(\|v_h\|^2 + 2 \sum_{F \in \mathcal{F}_{h,\Gamma}} \left(\frac{1}{\epsilon + \gamma h_F} \|[v_h]\|_{0,F}^2 + \gamma h_F \left\| \left\langle \kappa \frac{\partial v_h}{\partial \mathrm{n}} \right\rangle \right\|_{0,F}^2 \right) \right)^{1/2}.$$

The conclusion is reached thanks to Lemma 4.4, with $C_{\mathrm{ct}}^N = 2\max\{1, C_I\}$, independent of γ.

As regards the uniform coercivity, the choice (4.5) of β_F together with (4.3) yields that

$$a_h(v_h, v_h) \geq \sum_{K \in \mathcal{T}_h \setminus \mathcal{T}_{h,\Gamma}} \|\kappa^{1/2} \nabla v_h\|_{0,K}^2 + \sum_{K \in \mathcal{T}_{h,\Gamma}} (1 - 2\gamma C_I) \|\kappa^{1/2} \nabla v_h\|_{0,K}^2 + \|\alpha^{1/2} \nabla_\tau \langle v_h \rangle\|_{0,\Gamma}^2 + \frac{1}{2} \sum_{F \in \mathcal{F}_{h,\Gamma}} \frac{1}{\epsilon + \gamma h_F} \|[v_h]\|_{0,F}^2.$$

Choosing, for instance, $\gamma < \dfrac{1}{4C_I}$, we obtain the $|||\cdot|||_h$- coercivity with a constant $C_{\mathrm{cv}}^N = \dfrac{1}{2}$. □

Lemma 4.5 (Polynomial approximation in energy norm)**.** *For any $k \in \mathbb{N}^*$ and $v \in V_{\Gamma,0}^{k+1}$, there exists a constant $C_{\mathrm{ip}} > 0$ independent of h, ϵ, α, γ and κ such that:*

$$|||v - (\mathcal{I}_h^k)^* v|||_h \leq C_{\mathrm{ip}} h^k \left(\|\kappa^{1/2} v\|_{k+1,\Omega_1 \cup \Omega_2}^2 + \|(\alpha\epsilon)^{1/2} \langle v \rangle\|_{k+1,\Gamma}^2 + \sum_{F \in \mathcal{F}_{h,\Gamma}} \frac{h_F}{\gamma} \|[v]\|_{k+1,F}^2 \right)^{1/2}. \tag{4.6}$$

Moreover, one also has that:

$$|||v - (\mathcal{I}_h^k)^* v|||_h \leq C_{\mathrm{ip}} h^k \left(\|\kappa^{1/2} v\|_{k+1,\Omega_1 \cup \Omega_2}^2 + \frac{1}{\gamma} \|v\|_{k+1,\Omega_1 \cup \Omega_2}^2 + \|(\alpha\epsilon)^{1/2} \langle v \rangle\|_{k+1,\Gamma}^2 \right)^{1/2}. \tag{4.7}$$

Proof. With the same standard interpolation estimates as in Lemma 3.4, we immediately get that

$$|||v - (\mathcal{I}_h^k)^* v|||_h^2 \leq C_{\mathrm{ip}}^2 h^{2k} \left(\sum_{i=1}^{2} \sum_{K \in \mathcal{T}_h^i} \|\kappa_i^{1/2} v_i\|_{k+1,K}^2 + \sum_{F \in \mathcal{F}_{h,\Gamma}} \|(\alpha\epsilon)^{1/2} \langle v \rangle\|_{k+1,F}^2 \right) + C_{\mathrm{ip}}^2 h^{2k} \sum_{F \in \mathcal{F}_{h,\Gamma}} h_F^2 (\epsilon + \gamma h_F)^{-1} \|[v]\|_{k+1,F}^2.$$

Noting that $\gamma h_F (\epsilon + \gamma h_F)^{-1} < 1$, we immediately obtain (4.6). As regards estimate (4.7), it follows from the well-known trace inequality: there exists $C > 0$ such that for any $F \in \mathcal{F}_{h,\Gamma}$ with $F = \partial K_1 \cap \partial K_2$ and any $w_i \in \mathrm{H}^1(K_i)$ with $1 \leq i \leq 2$,

$$\frac{1}{\sqrt{h_F}} \|[w]\|_{0,F} \leq C \sum_{i=1}^{2} \left(\frac{1}{h_{K_i}} \|w_i\|_{0,K_i} + |w_i|_{1,K_i} \right).$$

Using next standard interpolation estimates, one gets for any $F \in \mathcal{F}_{h,\Gamma}$ that

$$\frac{1}{\epsilon + \gamma h_F} \|[v] - (\mathcal{I}_h^k)^* [v]]\|_{0,F}^2 \leq \frac{C_{\mathrm{ip}}^2}{\gamma} \sum_{i=1}^{2} h_{K_i}^{2k} |v_i|_{k+1,K_i}^2.$$

The announced estimate is obtained by summing upon $F \in \mathcal{F}_{h,\Gamma}$. □

The *a priori* error estimate for Nitsche's method is given below and follows from Céa's lemma.

Theorem 4.6 (Error estimate in energy norm)**.** *Let $k \in \mathbb{N}^*$, $u \in V_\Gamma^{k+1}$ the solution of* (2.2) *and u_h the solution of* (4.2)*. For γ sufficiently small, there exists a constant $C_{\rm e}^N = (1 + C_{\rm ct}^N/C_{\rm cv}^N)C_{\rm ip}$ independent of h, ϵ, α, γ and κ such that:*

$$|||\tilde{u} - \tilde{u}_h|||_h \leq C_{\rm e}^N h^k \left(\|\kappa^{1/2}\tilde{u}\|_{k+1,\Omega_1\cup\Omega_2}^2 + \|(\alpha\epsilon)^{1/2}\langle\tilde{u}\rangle\|_{k+1,\Gamma}^2 + \sum_{F\in\mathcal{F}_{h,\Gamma}} \frac{h_F}{\gamma}\|[\tilde{u}]\|_{k+1,F}^2 \right)^{1/2}, \tag{4.8}$$

where $\tilde{u} := u - \tilde{u}_{\rm D}$, $\tilde{u}_h := u_h - \tilde{u}_{{\rm D},h}$ with $\tilde{u}_{\rm D} \in {\rm H}^1(\Omega_1 \cup \Omega_2)$, $\tilde{u}_{{\rm D},h} \in P_h^k$ such that $\tilde{u}_{\rm D} = u_{\rm D}$, $\tilde{u}_{{\rm D},h} = u_{{\rm D},h}$ on $\Gamma_{\rm D}$ and $\tilde{u}_{\rm D} = \tilde{u}_{{\rm D},h} = 0$ on $\partial\Omega \setminus \Gamma_{\rm D}$. In addition, one has

$$|||\tilde{u} - \tilde{u}_h|||_h \leq C_{\rm e}^N h^k \left(\|\kappa^{1/2}\tilde{u}\|_{k+1,\Omega_1\cup\Omega_2}^2 + \frac{1}{\gamma}\|\tilde{u}\|_{k+1,\Omega_1\cup\Omega_2}^2 + \|(\alpha\epsilon)^{1/2}\langle\tilde{u}\rangle\|_{k+1,\Gamma}^2 \right)^{1/2}. \tag{4.9}$$

Remark 4.7. *One can note that, contrarily to the error estimate* (3.7) *of the first method, estimate* (4.8) *is robust for small values of ϵ. Indeed, if $\epsilon \leq \gamma h_F$, then $\dfrac{h_F}{\gamma} \leq \dfrac{h_F^2}{\epsilon}$ and moreover, the weight $\dfrac{h_F^2}{\epsilon}$ blows up as $\epsilon \to 0$.*

4.2 Numerical tests

In this subsection, we carry out some numerical experiments for the same test-cases as in Subsection 3.2, but using now the new Nitsche's type formulation. The goal is to illustrate that the energy error remains bounded for small values of ϵ, which is the main issue in the numerical examples of the previous section. The energy norm for Nitsche's formulation $e^N := |||\tilde{u} - \tilde{u}_h|||_h$ is also split into three terms, $(e^N)^2 = e_g^2 + e_\tau^2 + (e_j^N)^2$, where e_j^N now denotes the stabilised jump error on the interface,

$$(e_j^N)^2 := \sum_{F\in\mathcal{F}_{h,\Gamma}} (\epsilon + \gamma h_F)^{-1}\|[\tilde{u} - \tilde{u}_h]\|_{0,F}^2.$$

4.2.1 Convergence of the method with respect to the mesh size

We use a stabilisation parameter $\gamma = 10^{-1}$ for the first case and $\gamma = 5 \times 10^{-3}$ for the second case. We check numerically the error estimate given in Theorem 4.6 for the energy norm e^N, more precisely the convergence rate with respect to h at fixed ϵ.

The results are depicted in Figures 10 and 11 for the energy norm and the jump stabilized norm of the error, respectively. We observe that the results are similar to Figures 4 and 5. The orders of convergence are summarized in Table 2.

	Case 1	Case 2
e_g^N	0.98	1.04
e_τ^N	0.99	1.06
e_j^N	1.87	2.06
e^N	0.96	1.04

Table 2: Convergence rates of each error for Nitsche's method

4.2.2 Convergence with respect to ϵ

Let now h be fixed, for each test-case. We observe from Figure 12 that Nitsche's energy error e^N is bounded for small values of ϵ, contrarily to the energy error e that blows up. This is due to the fact that

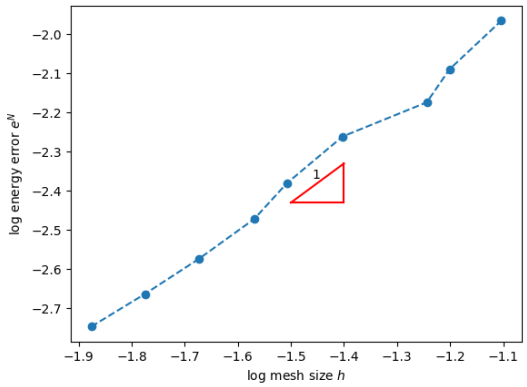

(a) Case 1 with $\epsilon = 10^{-2}$

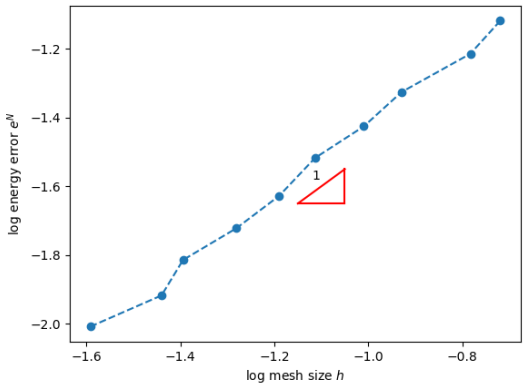

(b) Case 2 with $\epsilon = 1$

Figure 10: Logarithm plot of the energy error e^N with respect to the mesh size h

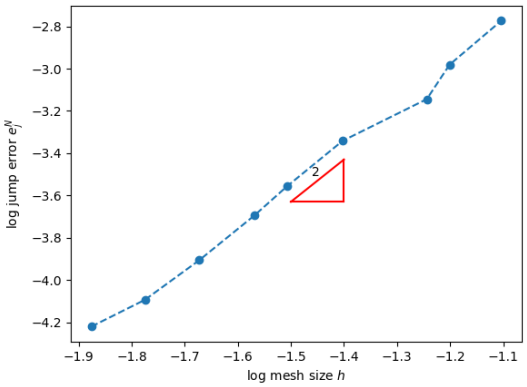

(a) Case 1 with $\epsilon = 10^{-2}$

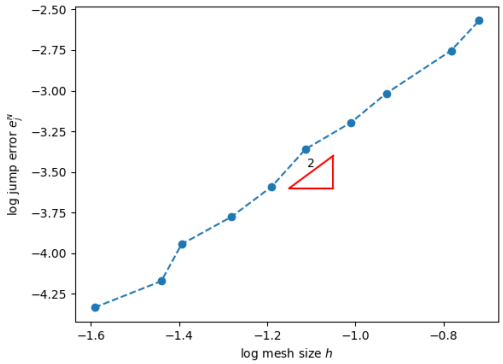

(b) Case 2 with $\epsilon = 1$

Figure 11: Logarithm plot of the jump error e_j^N with respect to the mesh size h

Nitsche's jump error is bounded, as shown in Figure 13. We note for both methods the good behaviour as ϵ decreases of the gradient and tangential errors, which are not affected by the $\frac{1}{\epsilon}$-term. The tangential gradient errors are plotted in Figure 14.

4.2.3 Conditioning

In Figure 15, we observe that the condition number of the Nitsche's method is bounded as ϵ tends towards 0, whereas the condition number of the first method increases, as highlighted in Subsection 3.2.4.

4.3 Application: use of iterative solvers

In this subsection we apply an iterative solver, more precisely the conjugate gradient method, to solve the linear system.

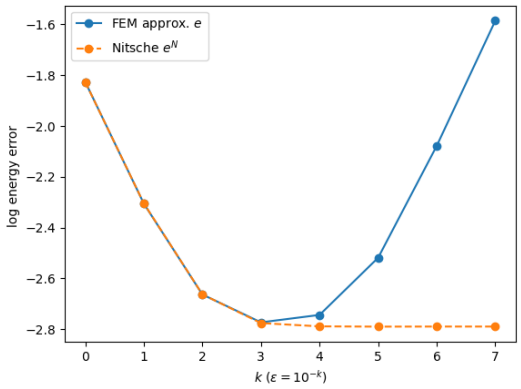

(a) Case 1 with $h = 1.6 \times 10^{-2}$

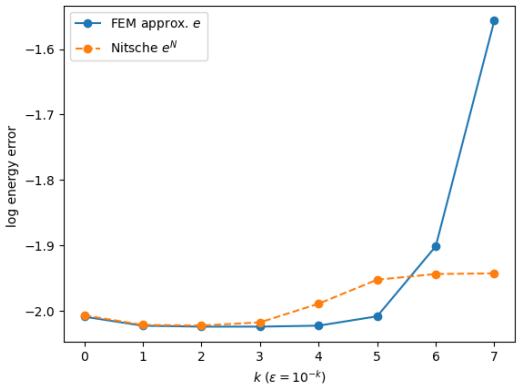

(b) Case 2 with $h = 2.5 \times 10^{-2}$

Figure 12: Logarithm plot with respect to ϵ of the energy errors $e = |||u - w_h|||$ and $e^N = |||u - u_h|||_h$, for FEM and Nitsche's methods respectively

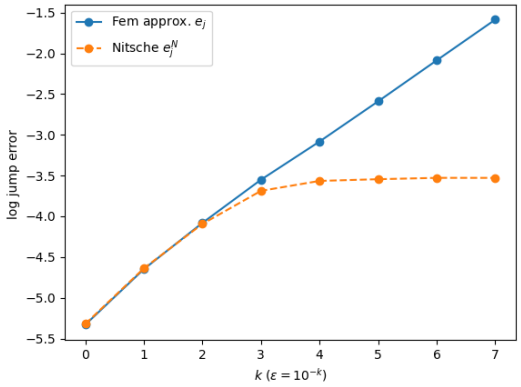

(a) Case 1 with $h = 1.6 \times 10^{-2}$

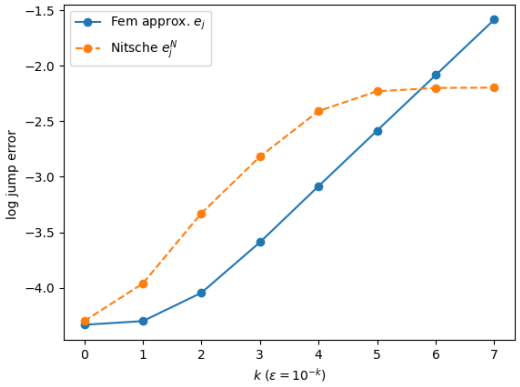

(b) Case 2 with $h = 2.5 \times 10^{-2}$

Figure 13: Logarithm plot with respect to ϵ of the jump errors $e_j = \|\epsilon^{-1/2}(u - w_h)\|_{0,\Gamma}$ and $e_j^N = (\sum_{F \in \mathcal{F}_{h,\Gamma}} \|(\epsilon + \gamma h_F)^{-1/2}(u - u_h)\|_{0,F}^2)^{1/2}$, for FEM and Nitsche's methods respectively

Firstly, we consider the test-case 1 as in Subsection 3.2.2, with fixed $h = 1.6 \times 10^{-2}$ and $\gamma = 10^{-1}$ for Nitsche's method. We let ϵ vary in order to see how the conditioning affects the performance of each method. We set the tolerance equal to 10^{-3} and the maximum number of iterations I equal to the matrix size, in this case $I = 11391$. Let $r := \|Ax - b\|$ the residual in the last iteration. We can see from Table 3 that as ϵ decreases, the number of iterations to reach the fixed tolerance with the first method increases; consequently, the errors increase too, since convergence is not reached in the last iterations. On the other hand, Table 4 shows that the number of iterations for Nitsche's method remains limited as ϵ goes to 0, and so do the errors.

Secondly, we consider the test-case 2 and we now set $tol = 10^{-4}$, $h = 2.5 \times 10^{-2}$ and $\gamma = 5 \times 10^{-3}$.

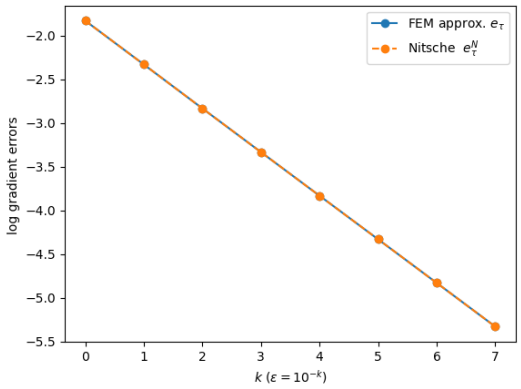

(a) Case 1 with $h = 1.6 \times 10^{-2}$

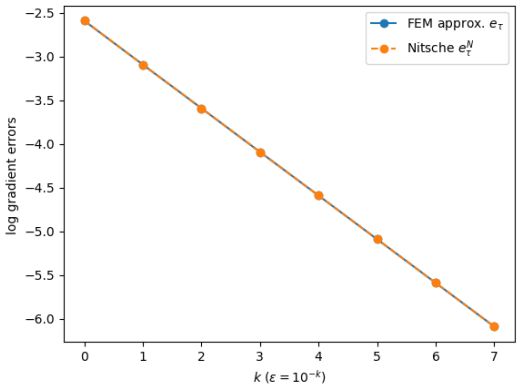

(b) Case 2 with $h = 2.5 \times 10^{-2}$

Figure 14: Logarithm plot with respect to ϵ of the tangential gradient errors $e_\tau = \|(\alpha\epsilon)^{1/2}\nabla_\tau(u - w_h)\|_{0,\Gamma}$ and $e_\tau^N = \|(\alpha\epsilon)^{1/2}\nabla_\tau(u - u_h)\|_{0,\Gamma}$, for FEM and Nitsche's methods respectively

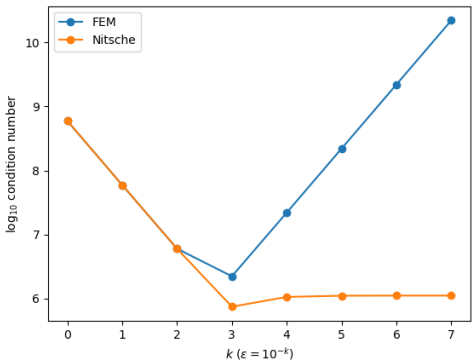

(a) Condition number of case 1 with $h = 3 \times 10^{-2}$

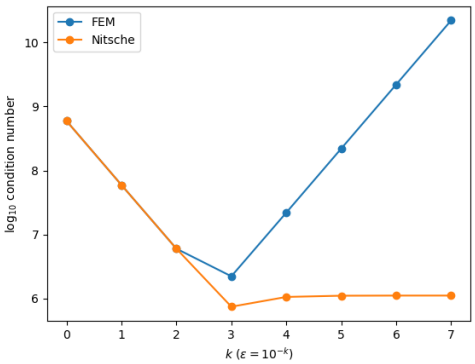

(b) Condition number of case 2 with $h = 5 \times 10^{-2}$

Figure 15: Logarithm plot with respect to ϵ of the condition number for the two methods

The matrix size is now 11005, so the maximum number of iterations is $I = 11005$. Tables 5 and 6 show similar results to the previous test-case.

Finally, we are interested to see how many iterations are necessary in order to attain convergence, without setting a maximum number of iterations. In Figure 16 we observe for both test-cases that the number of iterations in the FEM approximation (in blue) increases as ϵ decreases, whereas it remains bounded for Nitsche's method. Thus, the iterative solution of Nitsche's method converges faster than the one of the standard method.

ϵ	I	r	e	e_j	e_τ
10^0	11391	$5.6 \cdot 10^{-3}$	$1.2 \cdot 10^{-1}$	$1.3 \cdot 10^{-3}$	$7.8 \cdot 10^{-2}$
10^{-1}	11391	$1.9 \cdot 10^{-3}$	$3.4 \cdot 10^{-2}$	$8 \cdot 10^{-4}$	$1.3 \cdot 10^{-2}$
10^{-2}	6411	$9.5 \cdot 10^{-4}$	$1.7 \cdot 10^{-2}$	$1.1 \cdot 10^{-4}$	$1.5 \cdot 10^{-3}$
10^{-3}	2627	$9.1 \cdot 10^{-4}$	$1.9 \cdot 10^{-2}$	$2.9 \cdot 10^{-4}$	$5 \cdot 10^{-4}$
10^{-4}	5439	$9.3 \cdot 10^{-4}$	$1.8 \cdot 10^{-2}$	$8.9 \cdot 10^{-4}$	$1.9 \cdot 10^{-4}$
10^{-5}	8189	$8.9 \cdot 10^{-4}$	$1.9 \cdot 10^{-2}$	$2.7 \cdot 10^{-3}$	$6.1 \cdot 10^{-5}$
10^{-6}	11391	$1 \cdot 10^{-3}$	$1.8 \cdot 10^{-2}$	$9.5 \cdot 10^{-3}$	$3.5 \cdot 10^{-5}$
10^{-7}	11391	$1.8 \cdot 10^{-3}$	$4.1 \cdot 10^{-2}$	$2.7 \cdot 10^{-2}$	$2.2 \cdot 10^{-5}$

Table 3: Convergence history of conjugate gradient for case 1, using FEM approximation

ϵ	I	r	e^N	e_j^N	e_τ^N
10^0	11391	$5.4 \cdot 10^{-3}$	$1.3 \cdot 10^{-1}$	$1.3 \cdot 10^{-3}$	$7.8 \cdot 10^{-2}$
10^{-1}	11391	$1.6 \cdot 10^{-3}$	$3.3 \cdot 10^{-2}$	$5.2 \cdot 10^{-4}$	$1.3 \cdot 10^{-2}$
10^{-2}	6408	$9.9 \cdot 10^{-4}$	$1.7 \cdot 10^{-2}$	$1.2 \cdot 10^{-4}$	$1.5 \cdot 10^{-3}$
10^{-3}	2396	$9.3 \cdot 10^{-4}$	$2.3 \cdot 10^{-2}$	$2.1 \cdot 10^{-4}$	$5 \cdot 10^{-4}$
10^{-4}	2313	$9.2 \cdot 10^{-4}$	$2.1 \cdot 10^{-2}$	$3.1 \cdot 10^{-4}$	$1.9 \cdot 10^{-4}$
10^{-5}	2543	$9.4 \cdot 10^{-4}$	$1.8 \cdot 10^{-2}$	$3 \cdot 10^{-3}$	$6.1 \cdot 10^{-5}$
10^{-6}	2512	$9.6 \cdot 10^{-4}$	$1.9 \cdot 10^{-2}$	$3.7 \cdot 10^{-3}$	$3.5 \cdot 10^{-5}$
10^{-7}	2508	$9.9 \cdot 10^{-4}$	$1.9 \cdot 10^{-2}$	$3.4 \cdot 10^{-2}$	$2.2 \cdot 10^{-5}$

Table 4: Convergence history of conjugate gradient for case 1, using Nitsche's method

ϵ	I	r	e	e_j	e_τ
10^0	926	$9.1 \cdot 10^{-5}$	$9.8 \cdot 10^{-3}$	$7 \cdot 10^{-5}$	$2.5 \cdot 10^{-3}$
10^{-1}	434	$9.9 \cdot 10^{-5}$	$9.5 \cdot 10^{-3}$	$5.7 \cdot 10^{-5}$	$8 \cdot 10^{-4}$
10^{-2}	303	$8.7 \cdot 10^{-5}$	$9.5 \cdot 10^{-3}$	$9.6 \cdot 10^{-5}$	$2.5 \cdot 10^{-4}$
10^{-3}	492	$9.3 \cdot 10^{-5}$	$9.5 \cdot 10^{-3}$	$2.6 \cdot 10^{-4}$	$8 \cdot 10^{-5}$
10^{-4}	949	$8.8 \cdot 10^{-5}$	$9.5 \cdot 10^{-3}$	$7.9 \cdot 10^{-4}$	$2.5 \cdot 10^{-5}$
10^{-5}	1447	$9.5 \cdot 10^{-5}$	$9.8 \cdot 10^{-3}$	$2.5 \cdot 10^{-3}$	$8.1 \cdot 10^{-5}$
10^{-6}	1916	$9.5 \cdot 10^{-5}$	$1.3 \cdot 10^{-2}$	$8.3 \cdot 10^{-3}$	$2.5 \cdot 10^{-6}$
10^{-7}	2404	$9.2 \cdot 10^{-5}$	$2.7 \cdot 10^{-2}$	$2.6 \cdot 10^{-2}$	$8.1 \cdot 10^{-7}$

Table 5: Convergence history of conjugate gradient for case 2, using FEM approximation

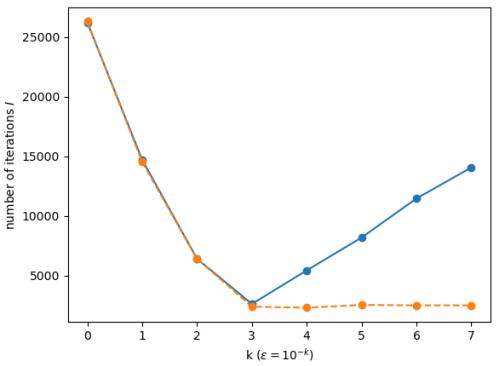

(a) Case 1
($h = 1.6 \times 10^{-2}$, $\gamma = 10^{-1}$, $tol = 10^{-3}$)

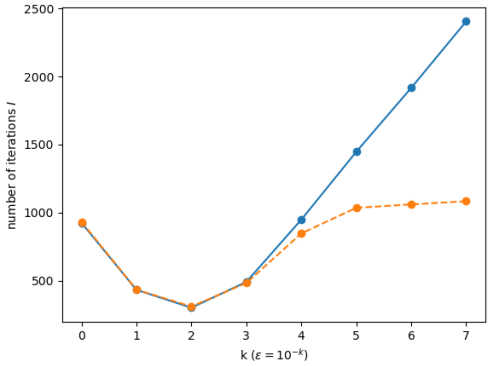

(b) Case 2
($h = 2.5 \times 10^{-2}$, $\gamma = 5 \times 10^{-3}$, $tol = 10^{-4}$)

Figure 16: Variation of the number of iterations with respect to ϵ for the txo methods

ϵ	I	r	e^N	e_j^N	e_τ^N
10^0	933	$9.4 \cdot 10^{-5}$	$9.8 \cdot 10^{-3}$	$7.9 \cdot 10^{-5}$	$2.5 \cdot 10^{-3}$
10^{-1}	435	$9.8 \cdot 10^{-5}$	$9.5 \cdot 10^{-3}$	$1.1 \cdot 10^{-4}$	$8 \cdot 10^{-4}$
10^{-2}	312	$8.5 \cdot 10^{-5}$	$9.5 \cdot 10^{-3}$	$4.7 \cdot 10^{-4}$	$2.5 \cdot 10^{-4}$
10^{-3}	484	$1 \cdot 10^{-4}$	$9.6 \cdot 10^{-3}$	$1.5 \cdot 10^{-3}$	$8 \cdot 10^{-5}$
10^{-4}	848	$1 \cdot 10^{-4}$	$1 \cdot 10^{-2}$	$3.9 \cdot 10^{-3}$	$2.5 \cdot 10^{-5}$
10^{-5}	1036	$9.3 \cdot 10^{-5}$	$1.1 \cdot 10^{-2}$	$6 \cdot 10^{-3}$	$8.1 \cdot 10^{-5}$
10^{-6}	1061	$9.9 \cdot 10^{-5}$	$1.1 \cdot 10^{-2}$	$6.3 \cdot 10^{-3}$	$2.5 \cdot 10^{-6}$
10^{-7}	1084	$9.5 \cdot 10^{-5}$	$1.1 \cdot 10^{-2}$	$6.3 \cdot 10^{-3}$	$8.1 \cdot 10^{-7}$

Table 6: Convergence history of conjugate gradient for case 2, using Nitsche's method

5 Conclusion and perspectives

In this paper, we have studied an extended Nitsche's type method for non-standard transmission problems with a mesh-aligned interface. We have shown optimal convergence with respect to h for a 2D piecewise linear approximation. Its main advantage, in comparison with a standard finite element method discontinuous at the interface, is the behaviour as ϵ decreases to 0 of its condition number, which remains bounded. This is particularly important if one uses iterative solvers to solve the linear system, especially in 3D problems with complex geometries.

In a future work, we plan to apply these techniques to shape optimisation in discontinuous interface problems, in particular to a thin film heat exchanger problem where ϵ is very small.

Acknowledgement

Rodrigo Zelada was partially funded by the National Agency for Research and Development (ANID) Scholarship Program BECA DOCTORADO NACIONAL 2021-21211704.

References

[1] G. Allaire, B. Bogosel, and M. Godoy. Shape optimization of an imperfect interface: steady-state heat diffusion. *Journal of Optimization Theory and Applications*, 191(1):169–201, 2021.

[2] G. Allaire, C. Dapogny, and P. Frey. A mesh evolution algorithm based on the level set method for geometry and topology optimization. *Structural and Multidisciplinary Optimization*, 48(4):711–715, 2013.

[3] C. Athanasiadis and I. G. Stratis. On some elliptic transmission problems. In *Annales Polonici Mathematici*, volume 63, pages 137–154, 1996.

[4] S. C. Brenner. *The mathematical theory of finite element methods*. Springer, 2008.

[5] D. Capatina, R. Luce, H. El-Otmany, and N. Barrau. Nxfem for solving non-standard transmission problems. In *Int. Conf." Numerical and Mathematical Modeling of Flow and Transport in Porous Media". Octobre 2014, Dubrovnik, Croatie*, 2014.

[6] D. Capatina, R. Luce, H. El-Otmany, and N. Barrau. Nitsche's extended finite element method for a fracture model in porous media. *Applicable Analysis*, 95(10):2224–2242, 2016.

[7] P. G. Ciarlet. *The finite element method for elliptic problems*. SIAM, 2002.

[8] D. A. Di Pietro and A. Ern. *Mathematical aspects of discontinuous Galerkin methods*, volume 69. Springer Science & Business Media, 2011.

[9] M. Dryja. On discontinuous galerkin methods for elliptic problems with discontinuous coefficients. *Computational Methods in Applied Mathematics*, 3(1):76–85, 2003.

[10] A. Hansbo and P. Hansbo. An unfitted finite element method, based on nitsche's method, for elliptic interface problems. *Computer methods in applied mechanics and engineering*, 191(47-48):5537–5552, 2002.

[11] A. Henrot and M. Pierre. *Variation et optimisation de formes: une analyse géométrique*, volume 48. Springer Science & Business Media, 2006.

[12] M. Juntunen and R. Stenberg. Nitsche's method for general boundary conditions. *Mathematics of computation*, 78(267):1353–1374, 2009.

[13] T. Kashiwabara, C. M. Colciago, L. Dedè, and A. Quarteroni. Well-posedness, regularity, and convergence analysis of the finite element approximation of a generalized robin boundary value problem. *SIAM Journal on Numerical Analysis*, 53(1):105–126, 2015.

[14] J. Nitsche. Über ein Variationsprinzip zur Lösung von Dirichlet-Problemen bei Verwendung von Teilräumen, die keinen Randbedingungen unterworfen sind. In *Abhandlungen aus dem mathematischen Seminar der Universität Hamburg*, volume 36, pages 9–15. Springer, 1971.

[15] A. D. Wentzell. On boundary conditions for multi-dimensional diffusion processes. *Theory Probab. Appl*, 4(2):164–177, 1959.